Medina, V., Loi, D., Rombouts, P. & Hernandez, L. (21-25 May, 2023). *Analysis of in-band Spurious Tones of VCO-based Analog Filters and Mitigation Techniques* [proceedings]. 2023 IEEE International Symposium on Circuits and Systems (ISCAS), Monterey, USA.

DOI: 10.1109/ISCAS46773.2023.10181860

Analysis of in-band Spurious Tones of VCO-based Analog Filters and Mitigation Techniques

Victor Medina
Electronic Tech. Dept.
Carlos III University
Leganes, Spain
vmedina@ing.uc3m.es

Dante Loi
Electronic Tech. Dept.
Carlos III University
Leganes, Spain
dloi@ing.uc3m.es

Pieter Rombouts
ELIS
Ghent University
Ghent, Belgium
pieter.rombouts@ugent.be

Luis Hernandez
Electronic Tech. Dept.
Carlos III University
Leganes, Spain
luish@ing.uc3m.es

***Abstract*—Recently VCO-based filters have been used to implement feature extraction in voice recognition systems. Typically implemented filter structures embed the VCOs in a feedback loop. In these implementations, harmonic distortion has been observed in the output signal. This harmonic distortion has been attributed to ring oscillator nonlinearity but its origin stems from a system level problem. In this manuscript we will analyze this problem by looking at the cross modulation of Pulse Frequency Modulation (PFM) side-bands and we will explain how this creates the previously misunderstood harmonic distortion. Moreover, we will propose efficient techniques to mitigate these harmonic components and show that they can easily be implemented in hardware.**

***Index Terms*—VCO-ADC, Pulse Frequency Modulation, Analog filters, Voice feature extraction**

I. Introduction

Edge AI applications dealing with voice processing often require efficient band-pass audio filters for feature extraction. These filters have noise and distortion requirements of around 50 dB SNDR. In despite of this relatively modest specification, they still represent a big share of the power and/or of the area budget. Several structures have been published in the recent years, ranging from quite conventional continuous time analog filter solutions [1], switched capacitor [2], multiplexed time domain [3] to fully digital approaches [4]. An alternative solution is based on VCO-based filtering techniques, of which some possible implementations were demonstrated in [5], [6]. Also, a more general mathematical description based on PFM was already given in [7] where it was shown that the filter can easily be implemented by asynchronous digital logic consisting of digital primitives such as counters and flip-flops.

Using such VCO-based filters, an efficient feature extraction architecture was proposed in [8] and implemented in [9], [10]. Compared to analog solutions, the VCO-based approach is free of area consuming elements (e.g. large capacitors), while being much more power efficient than fully digital solutions.

However, VCO-based filters have a system level problem that has not been analyzed so far and sometimes has been partially attributed to circuit mismatch and non linearity (and hence was considered a hardware implementation issue). The phenomenon is that whenever we have a loop around a VCO, which uses a frequency modulated signal as input, harmonic distortion components appear in the output signal.

This paper was supported by program H2020-MSCA-ITN-2020 grant Nr. 956601 and project PID2020-118804RB-I00 of the Spanish Agency of Research (AEI) and by FWO-Vlaanderen.

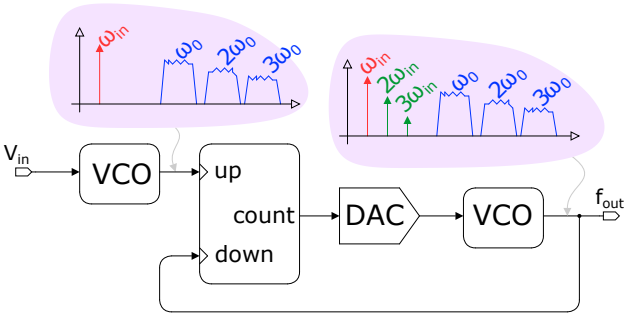

Fig. 1. Basic VCO-based low-pass filtering stage, the -3 dB cut-off frequency is the loop-gain $\omega_c = K_D \times K_V$, harmonic distortion at the output is present regardless of the hardware implementation of the oscillators.

To illustrate the problem, Figure 1 shows the system level diagram of a VCO-based first order low-pass filter with cutoff frequency ω_c. It consists of an input VCO with gain K_V that encodes the signal V_{in} from an analog source (for instance voice from a microphone) into a PFM signal. Then this signal drives a loop containing another VCO with the same gain that tracks the frequency of the first VCO via an up/down counter and a DAC with gain K_D. The -3 dB cut-off frequency of the filter is calculated as $\omega_c = K_D \times K_V$. Assuming a sinusoidal input, the input PFM spectrum after the first VCO contains the input signal plus modulation side-bands at the harmonics of the VCO rest frequency $\omega_0/2\pi$. In principle, the loop VCO should respond with a first order low-pass filtered version of the input. A behavioral simulation, even without any circuit impairments, shows that this PFM signal contains in-band harmonics that degrade the SNDR at the output of the filter. This paper tackles this problem from the signal theory point of view, revealing a distortion mechanism which is inherent to the PFM encoding process embedded in the filter. In this paper, we will base our discussion on a simple low-pass filter. But as we will explain, the phenomenon occurs always when there is a feedback loop with a PFM encoded input signal and a fed back signal which is also PFM encoded. Hence it will also occur in band-pass and high-pass filters that are based on feedback.

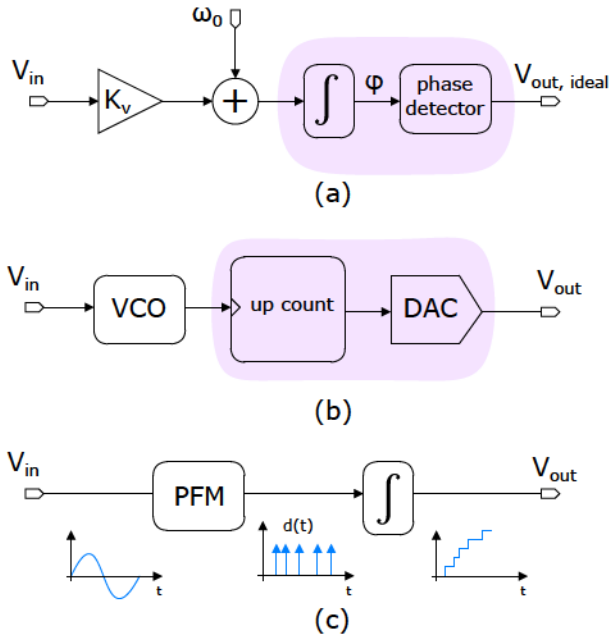

Fig. 2. (a) Phase domain model of a VCO integrator and (b) practical implementation with a phase detector consisting of a generalized PFD, (c) PFM based model of the practical VCO integrator.

The paper is organized in three sections. Section II describes the operation of a VCO-based filter using the PFM representation theory to investigate the spectrum of the signals inside of such a filter loop. Then, Section III simulates the non-linearity effect in a filter and uses a Discrete Fourier Series analysis to represent the signals within the loop and the root cause of the distortion. Finally Section IV proposes some simple mitigation techniques to tackle the distortion in a practical filter.

II. VCO-BASED FILTERS

The well established phase-domain model of a VCO displayed in Fig. 2(a), provides a direct equivalence between a VCO and an infinite DC gain integrator, since the phase of the oscillator is given by the time integral of the input dependent frequency of the VCO [5]. However, most practically relevant VCOs are pseudo-digital ring oscillators [11]–[13], which do not provide access to the instantaneous phase of the oscillator. Instead, the only available information is the position of edges of the output waveform. In a theoretical VCO analysis, this problem is solved by adding an idealized block, the *phase detector*, that provides access to the internal phase, leading to an ideal output signal $V_{\text{out,ideal}}$. A very attractive practical realization is based on counting the VCO edges, and is shown in Fig. 2(b). Note that a multi-phase ring oscillator can be considered as a single phase one equipped with a multi-bit counter [11], up to a frequency adjustment. In the special case where the up/down counter of Fig. 1 can only have the output values -1, 0, and 1, it collapses into the well-known Phase Frequency Detector (PFD), ubiquitously used in PLLs. Nevertheless, the output signal V_{out} of this practical structure

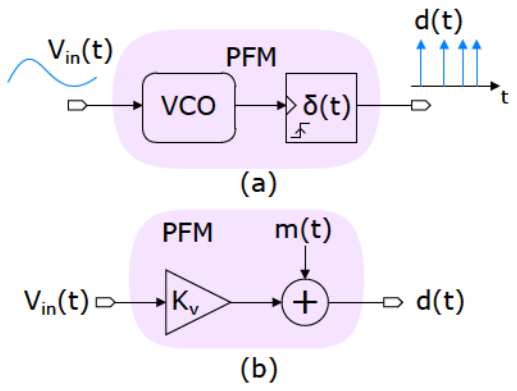

Fig. 3. (a) a VCO with only edge information is a PFM. (b) Model of a PFM as a linear gain with an injection of high-frequency modulation spurs.

is not equal to that of the ideal structure of Fig. 2(a). Until recently, this impeded exact understanding of this structure.

As outlined in [14], a VCO with only edge information available is strictly equivalent to a PFM modulator (see Fig. 3(a)) producing a Dirac delta stream of which any two consecutive times of occurrence t_{k-1}, and t_k are related by:

$$\int_{t_{k-1}}^{t_k} \left[\frac{\omega_0}{2\pi} + K_V \cdot V_{in}(\tau)\right] \mathrm{d}\tau = 1 \tag{1}$$

$$d(t) = \sum_{k=1}^{N} \delta(t - t_k), \quad t_N < t < t_{N+1} \tag{2}$$

where N is the number of full cycles the oscillator has completed up to time t_N. The frequency behavior of a PFM signal is extensively studied in [15]. In particular it has been shown that for sinusoidal inputs, the PFM signal $d(t)$ can be written as two components: first a component proportional to the input signal, and second, a modulation component $m(t)$ located at higher frequencies (centered around integer multiples of the VCO rest frequency $\omega_0/2\pi$). This was exploited in [14] to come up with the model of Fig. 3(b). Here the modulation component $m(t)$ is considered as a spurious error. For the operation of a VCO-based filter, the idea is that these undesired modulation spurs $m(t)$ are out-of-band and do not interfere with the desired base-band signals contained in the PFM spectra.

Revisiting the practical implementation of Fig. 2(b), it becomes clear that within the PFM interpretation the counter output is strictly equivalent to an integration of the PFM output signal $d(t)$. This leads to the equivalent diagram of a practical VCO integrator shown in Fig. 2(c), where also the corresponding time domain wave forms are represented. By embedding one (or more) of such an integrator in a feedback loop, practical filters such as the one shown in Fig. 1, are obtained.

The equivalence between Fig. 2(b) and Fig. 2(c) can also be proven analytically. On one hand, we can calculate the integral

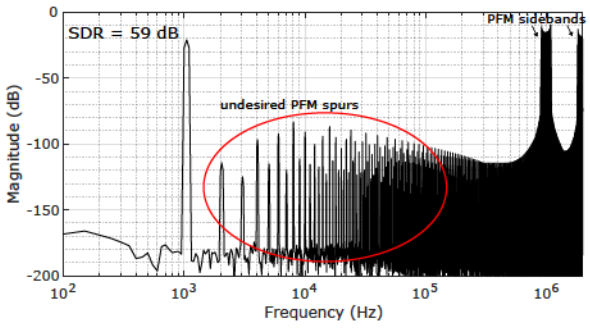

Fig. 4. Simulated output spectrum for a VCO-Based low-pass filter with the considered parameters.

of the PFM signal d(t) up to the last Dirac impulse generated at time t_N:

$$V_{out}(t_N) = \int_0^{t_N} \sum_{k=1}^{N} \delta(\tau - t_k)\, \mathrm{d}\tau = \sum_{k=1}^{N} u(t_N - t_k) = N \quad (3)$$

On the other hand, we can calculate the integral of the input signal V_{in} up to t_N and apply (1) to see that both equations match. Note that we have defined $V'_{in} = \omega_0/(2\pi K_v) + V_{in}$ as V_{in} with a DC offset to account for the rest frequency ω_0:

$$\int_0^{t_N} K_V \cdot V'_{in}(\tau)\, \mathrm{d}\tau = \sum_{k=1}^{N} \int_{t_{k-1}}^{t_N} K_V \cdot V'_{in}(\tau)\, \mathrm{d}\tau = N \quad (4)$$

$$\int_0^{t_N} d(\tau)\, \mathrm{d}\tau = \int_0^{t_N} K_V \cdot V'_{in}(\tau)\, \mathrm{d}\tau \quad (5)$$

III. In-band Spurious Tones in VCO-based Filters

Figure 4 shows the output spectrum of the filter of Fig. 1, for the simulation parameters reported in table I, where the Signal to Distortion Ratio (SDR) is 59 dB for a bandwith of 20 kHz. The considered PFM block only reacts to rising edges and its output is normalized to keep the same amplitude level for the input tone. We can observe that the output does not only contain the filtered input tone and the typical side-bands [15], but also harmonics near the input tone and also tones smeared between the different side-bands. Based on the implementation of a VCO-based low pass filter, we investigate this output spectrum according to the PFM theory.

TABLE I
Simulation parameters

Input Tone		VCO/PFM		Filter
$\omega_{in}/2\pi$	A_{in}	$\omega_0/2\pi$	K_V	$\omega_c/2\pi$
1 kHz	9 mV	1 MHz	1 MHz/V	10 kHz

Figure 5 presents four low-pass simplified equivalent systems, ranging from a system composed by just an ideal integrator up to the one of Fig. 1, passing by different variants which insert PFM blocks in the signal path. The outputs of a) and b) can be analytically calculated for sinusoidal inputs. The signals that compose the output of system b) present only side-bands around multiples of the rest frequency. It is clear that

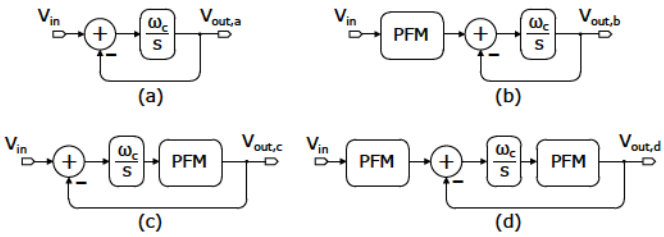

Fig. 5. Equivalent low-pass filters, from (a) an ideal integrator to (d) a VCO-based low-pass filter.

systems b) and c) are not practical to implement in hardware; however, system c) comes in handy when studying the output spectrum of our study case, as we can isolate the effect of having the PFM block in the loop without spurious injection at the input stage. A simulated output spectrum of system c) is shown in Fig. 6. In this case some harmonics are still present, but they have a low magnitude. Therefore it looks like the strong degradation seen in system d) is due to both input and in-loop PFM blocks.

To obtain the analytical output spectrum for either system c) or d) is not an easy task. Nonetheless, we can approximate system d) by means of the open-loop system depicted in Fig. 7. We feed the output of system b) into a second PFM2 modulator. The output of such simplified topology can be analytically calculated using the equations developed in [16] but still this results in several infinite sums. To obtain analytical results, we will make the following approximations for the input modulator, PFM1: first, we only consider the first modulation side-band (near the rest frequency ω_0). This is justified because the modulation sidebands at higher frequency are attenuated by the filter. Furthermore, we will only take a limited number of modulation components into account (arbitrarily chosen as 7). Together with the input tone this gives 8 frequency components represented by the vector $\boldsymbol{f_{sb}}$:

$$\boldsymbol{f_{sb}} = [f_{in}, f_o - 3f_{in}, \cdots, f_o, \cdots, f_o + 3f_{in}]. \quad (6)$$

The same vectorial notation can be used for its magnitudes and initial phases, $\boldsymbol{A_{sb}}$ and $\boldsymbol{\theta_{sb}}$. Now, the expression for the side-bands $M(f)$ of PFM2 is given by:

$$M(f) = f_0 \sum_{q=1}^{\infty} \sum_{r_1=-\infty}^{\infty} \cdots \sum_{r_8=-\infty}^{\infty} \prod_{k=1}^{8} J_{r_k}\left(q \frac{A_{sb_k} K_V}{f_{sb_k}}\right)$$
$$\cdot \left(1 + \frac{\boldsymbol{r} \cdot \boldsymbol{f_{sb}}}{q f_0}\right) \cdot e^{j\left[\boldsymbol{r} \cdot \boldsymbol{\theta_{sb}} - \sum_p q \frac{A_{sb_p} K_V}{f_{sb_p}} \sin \theta_{sb_p}\right]}$$
$$\cdot \{\delta[f + (q f_o + \boldsymbol{r} \cdot \boldsymbol{f_{sb}})] + \delta[f - (q f_o + \boldsymbol{r} \cdot \boldsymbol{f_{sb}})]\}, \quad (7)$$

$$\exists q, \boldsymbol{r} \text{ such that } (q f_o + \boldsymbol{r} \cdot \boldsymbol{f_{sb}}) = n f_{in}, n \in \mathbb{N}. \quad (8)$$

This equation expresses that not only the input signal, but also components of the first side-band generated by PFM are fed into PFM2. These components (from PFM1) are then in turn modulated by the PFM2. Observing (8) we may see that there are multiple combination of values of $\boldsymbol{r}$ that result in base band harmonic distortion components. E.g. the contribution of the

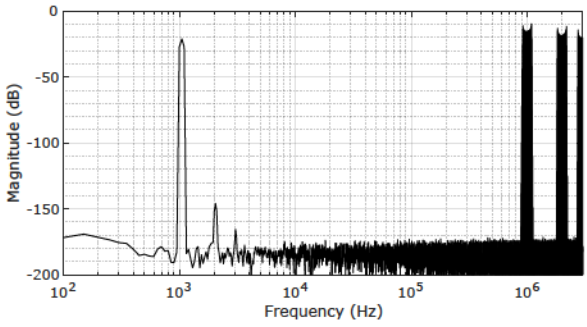

Fig. 6. Simulated output spectrum for Fig. 5 (c).

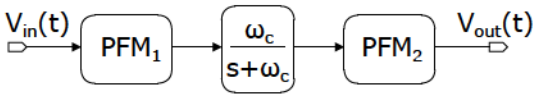

Fig. 7. Simplified version of system (d) in open-loop configuration, delivering a qualitatively comparable response.

component with $q = 1$ and $r \cdot f_{sb} = f_0 + 2f_{in}$ will give an harmonic distortion component at $2f_{in}$.

Note that the mechanism is *cross* modulation and hence, only occurs when high-frequency side-band tones of a PFM signal modulate another similar PFM signal.

Even for this case in which we are considering just a few components driving PFM2, analyzing (7) becomes complicated. Instead of an analytical calculation, we have done a behavioral simulation, (shown in Fig. 8), proving the insight given by (7). Even though this approximation does not yield the exact same spectrum as Fig. 4, it shares the same behaviour with respect to the harmonics.

IV. Mitigation Techniques

Given the fact that low frequency spectrum degradation is due to cross-modulation between side-bands generated in a PFM modulator, there are two obvious ways to tackle the problem: 1) by pushing away the side-bands to higher frequencies where the loop integration produces more attenuation. This correspond to increasing the effective VCO rest frequency, which can be done by designing a faster VCO or alternatively by multiple phases of a ring oscillator VCO [14] and 2) by placing a passive low-pass filter at the input of the in-loop PFM modulator with cutoff frequency ω_f which further attenuates the PFM side-bands. Technique 1) comes at the expense of an increase in power consumption, and/or area. Technique 2) comes at the expense of an extra capacitor. Figure 9 black, shows a simulation where the effective VCO rest frequency is increased by a factor of 15. For this case, the improvement in SDR was 44 dB. Method 2) is also a viable solution and for a cutoff frequency of 125 kHz, it yields an improvement of 21 dB. However, we can consider a trade-off with regard to the bandwidth ω_f of the extra in-loop filter. The bandwidth should be much larger than the bandwidth ω_c of the actual filter such that the extra in-loop filter negligibly effects the nominal filtering operation of the overall system. A second reason to

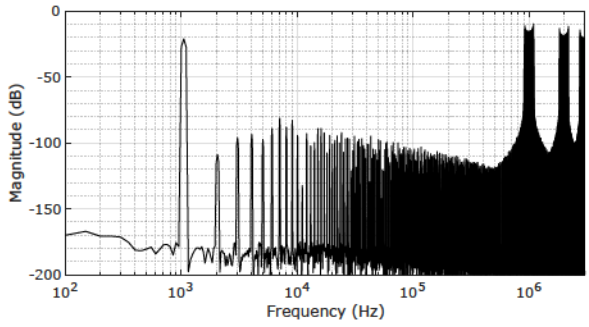

Fig. 8. Simulated output spectrum for the simplified open-loop system depicted in Fig. 7.

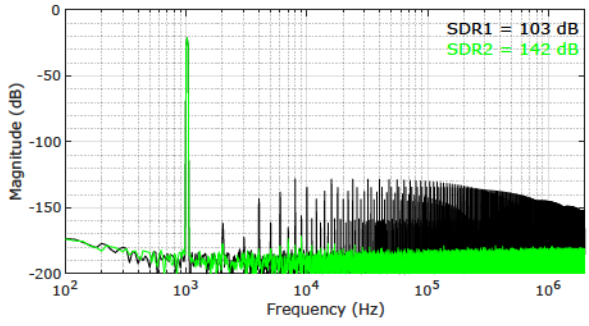

Fig. 9. Simulated output spectrum when using a multi-phase solution with an equivalent $f_{0\ \ eq} = 15 \cdot f_0$ (black), and when combining multi-phase with a low-pass filter within the loop (green).

make ω_f large is that we do not want to use large capacitors. But on the other hand, the bandwidth of the extra filter should be low for this mitigation technique to be effective. The most effective approach is combining the two techniques, which is illustrated in the green curve of Fig. 9 where an extra filter low pass filter in the loop with a cutoff of 125 kHz was added. This method effectively removes the harmonic content and yields a SDR of 142 dB.

V. Conclusion

We have explained how a PFM interpretation can be applied to enable a more complete understanding of VCO-based filters. This interpretation gives insight in the nature of the high-frequency out-of-band modulation spurs that occur in such a VCO-based filter. Thanks to this insight, we have identified an inherent distortion mechanism. Unfortunately this situation always occurs when a VCO-integrator is embedded in a feedback loop as will normally be the case for a VCO-based filter. Hence this problem can be considered inherent to VCO-based filtering.Fortunately, the PFM interpretation also provides the recipe to mitigate the problem: i.e. attenuate the high frequency modulation spurs before they are applied to a VCO integrator. A very simple but effective technique to do this is by preceding a VCO integrator by a lowpass filter with a cutoff frequency that is lower than the VCO oscillation frequency.

REFERENCES

[1] M. Yang, C.-H. Yeh, Y. Zhou, J. P. Cerqueira, A. A. Lazar, and M. Seok, "A 1 μW voice activity detector using analog feature extraction and digital deep neural network," in *Proc. IEEE Int. Solid State Circuits Conf. (ISSCC)*, 2018, pp. 346–348.

[2] K. M. H. Badami, S. Lauwereins, W. Meert, and M. Verhelst, "A 90 nm CMOS, 6 μW Power-Proportional Acoustic Sensing Frontend for Voice Activity Detection," *IEEE J. Solid-State Circuits*, vol. 51, no. 1, pp. 291–302, 2016.

[3] M. Cho, S. Oh, Z. Shi, J. Lim, Y. Kim, S. Jeong, Y. Chen, D. Blaauw, H.-S. Kim, and D. Sylvester, "17.2 A 142nW Voice and Acoustic Activity Detection Chip for mm-Scale Sensor Nodes Using Time-Interleaved Mixer-Based Frequency Scanning," in *Proc. IEEE Int. Solid State Circuits Conf. (ISSCC)*, 2019, pp. 278–280.

[4] J. S. P. Giraldo, S. Lauwereins, K. Badami, and M. Verhelst, "Vocell: A 65-nm Speech-Triggered Wake-Up SoC for 10-μW Keyword Spotting and Speaker Verification," *IEEE J. Solid-State Circuits*, vol. 55, no. 4, pp. 868–878, 2020.

[5] B. Drost, M. Talegaonkar, and P. K. Hanumolu, "Analog Filter Design Using Ring Oscillator Integrators," *IEEE J. Solid-State Circuits*, vol. 47, no. 12, pp. 3120–3129, 2012.

[6] L. B. Leene and T. G. Constandinou, "Time domain processing techniques using ring oscillator-based filter structures," *IEEE Transactions on Circuits and Systems I: Regular Papers*, vol. 64, no. 12, pp. 3003–3012, 2017.

[7] L. Hernandez, E. Gutierrez, and F. Cardes, "Frequency-encoded integrators applied to filtering and sigma-delta modulation," in *Proc. IEEE Int. Symp. Circuits and Syst. (ISCAS)*, 2016, pp. 478–481.

[8] E. Gutierrez, C. Perez, F. Hernandez, and L. Hernandez, "VCO-based Feature Extraction Architecture for Low Power Speech Recognition Applications," in *Proc. IEEE Midwest Symp. Circuits and Syst. (MWSCAS)*, 2019, pp. 1175–1178.

[9] N. Goux, J.-B. Casanova, G. Pillonnet, and F. Badets, "A 6-nw 0.0013-mm² ilo bandpass filter for time-based feature extraction," *IEEE Solid-State Circuits Letters*, vol. 3, pp. 306–309, 2020.

[10] K. Kim, C. Gao, R. Graça, I. Kiselev, H.-J. Yoo, T. Delbruck, and S.-C. Liu, "A 23- μW Keyword Spotting IC With Ring-Oscillator-Based Time-Domain Feature Extraction," *IEEE J. Solid-State Circuits*, pp. 1–14, 2022.

[11] G. G. Gielen, L. Hernandez, and P. Rombouts, "Time-Encoding Analog-to-Digital Converters: Bridging the Analog Gap to Advanced Digital CMOS-Part 1: Basic Principles," *IEEE Solid-State Circuits Magazine*, vol. 12, no. 2, pp. 47–55, 2020.

[12] ——, "Time-Encoding Analog-to-Digital Converters: Bridging the Analog Gap to Advanced Digital CMOS-Part 2: Architectures and Circuits," *IEEE Solid-State Circuits Magazine*, vol. 12, no. 3, pp. 18–27, 2020.

[13] J. Borgmans, R. Riem, and P. Rombouts, "The Analog Behavior of Pseudo Digital Ring Oscillators Used in VCO ADCs," *IEEE Trans. Circuits Syst.-I: Regular Papers*, vol. 68, no. 7, pp. 2827–2840, 2021.

[14] E. Gutierrez, L. Hernandez, F. Cardes, and P. Rombouts, "A Pulse Frequency Modulation Interpretation of VCOs Enabling VCO-ADC Architectures With Extended Noise Shaping," *IEEE Trans. Circuits Syst.-I: Regular Papers*, vol. 65, no. 2, pp. 444–457, Feb 2018.

[15] E. J. Bayly, "Spectral analysis of pulse frequency modulation in the nervous systems," *IEEE Transactions on Biomedical Engineering*, vol. BME-15, no. 4, pp. 257–265, 1968.

[16] M. Nakao, M. Norimatsu, Y. Mizutani, and M. Yamamoto, "Spectral distortion properties of the integral pulse frequency modulation model," *IEEE Transactions on Biomedical Engineering*, vol. 44, no. 5, pp. 419–426, 1997.